15 years of SAR Interferometry

S. STRAMONDO

INGV - Istituto Nazionale di Geofisica e Vulcanologia, Roma, Italy

(Received: May 04, 2007; accepted: August 02, 2007)

ABSTRACT Since the end of the 1980s a technique based on the use of Synthetic Aperture Radar (SAR) data from Earth-orbiting instruments has been developed. The approach, known as SAR Interferometry (InSAR) is able to provide accurate measurements of the Earth's surface deformations due to geological and geophysical phenomena, as earthquakes, landslides and volcanic eruptions. In less than two decades the InSAR technique has spread through a wide range of Earth Science fields. During these years a huge amount of applications were made and a vast number of theoretical and applicative manuscripts are available in literature today. Recent improvements in InSAR lead to the development of a new approach, referred to as Advanced InSAR (A-InSAR) techniques, which are addressed to the monitoring of slow movements in time. This work does not attempt to be a comprehensive review of the theory and applications of InSAR and A-InSAR, but it would like to provide a basic overview of these techniques.

1. Introduction

Synthetic Aperture Radar (SAR) exploits satellite orbit information to obtain a spatial resolution which is much higher (tens of meters) than standard radar systems. SAR processing significantly improves the resolution of point targets in both the cross-track (range) and along-track (azimuth) direction by focusing the raw radar echoes (Elachi, 1988; Curlander and McDonough, 1991). The SAR signal processing technique referred to as SAR Interferometry (InSAR) is widely used in seismology, volcanology, hydrogeology and landslide studies. It is not far from the truth to say that InSAR revolutionized a considerable part of Earth Sciences. In fact, in the last 15 years InSAR has shown to have unique capabilities for mapping the topography and the deformation of the Earth's surface. The InSAR approach is based on extracting the phase component of SAR data to compute the pixel-by-pixel difference of the SAR signal relative to a specific area and acquired from nearby geometric conditions. The interferogram, i.e. the result of the interferometric processing, contains the measurement of the sensor to the target distance and of any possible change distance.

The aim of this work is far from providing an exhaustive review of the InSAR theory and applications. However, it would like to give an overview on this technique and on the most relevant results.

InSAR early studies used Seasat satellite data to detect vertical motions of irrigated fields caused by soil swelling in the Imperial Valley, California. Gabriel *et al*. (1989) affirmed that InSAR "can measure accurately extremely small changes in terrain over the large swaths associated with SAR imaging, especially since the sensor can work at night and through clouds or precipitations". At the initial stage, InSAR showed promising capabilities which were later confirmed by a huge number of significative results.

InSAR obtained the highest number of results in seismology fieldwork. Since the early 1990s, the InSAR technique has been exploited to study the surface displacement due to moderate-to-strong earthquakes (Massonnet *et al*., 1993; Peltzer and Rosen, 1995; Stramondo *et al*., 1999; Reilinger *et al*., 2000). Anyway a number of papers devoted to InSAR applications have already been published such as these concerning the effect of volcanic eruptions (Massonnet *et al*., 1995; Jónsson *et al*., 1999; Salvi *et al*., 2004) and the ground subsidence due to fluid extraction (Massonnet *et al*., 1997; Galloway *et al*., 1998; Amelung *et al*., 1999), for instance. More generally, InSAR has demonstrated its capability of providing an accurate measurment of surface deformations from space, as it operates with all kinds of atmospheric conditions (weather indipendent), day and night (time indipendent). Together with these factors, the wide coverage of each image, the global coverage, the repetitiveness of the observations makes InSAR a valuable tool for surface deformation measurement and monitoring.

Since 2001, the main interest of researchers shifted towards the investigation of the temporal evolution of surface deformation phenomena. Parallelly, a remarkable improvement has been the development of an innovative approach based on the use of a large data set of SAR images over the same area. The Advanced InSAR (A-InSAR) techniques overcome the limitations of the standard InSAR, as the deformation modeling, the more accurate measurement of deformations through the better estimation of topography and atmospheric phases.

Various research groups developed InSAR multitemporal approaches (Ferretti *et al*., 2000; Berardino *et al*., 2002; Mora *et al*., 2003; Usai, 2003; Werner *et al*., 2003; Hooper *et al*., 2004; Crosetto *et al*., 2005).

Few words about the SAR sensors available for InSAR. None of the former radar image satellites were planned for interferometric scopes. Anyway, the quality and quantity of the relevant results addressed towards their use for InSAR. Since 1992, with the launch of ERS-1 (and, later in 1995, ERS-2) the European Space Agency (ESA) made C-Band sensors available. ERS-1 & 2 were followed by the Envisat Advanced SAR (ASAR) in 2001. The Canadian Space Agency has developed the C-Band Radarsat-1 and in 2007 Radarsat-2. As far as the Japanese Space Agency is concerned the L-Band JERS1 and, recently, ALOS satellites are available. Very recently the German Space Agency (DLR) and the Italian Space Agency (ASI) addressed their efforts toward the development of the X-Band SAR, respectively with the Terrasar-X and the CosmoSkymed missions (the latter is a constellation).

2. InSAR basic concepts

The SAR image contains a two-dimensional record of both the amplitudes and the phases of the returns from targets within the imaging area. The amplitude stands for the reflectivity while the phase is a term proportional to the sensor-to-target distance and records possible surface movements (Fig. 1).

Two SAR satellite images can be combined to generate an interferogram. In particular, the phase difference of two images with the same viewpoint can accurately measure any shifts of the returned phase, thus computing the Earth's surface movement towards or away from the satellite. Moving along their orbit the SAR sensors can simultaneously acquire the investigated scene, or can look at the target at different times if a single antenna is available and the satellite passes the investigated area

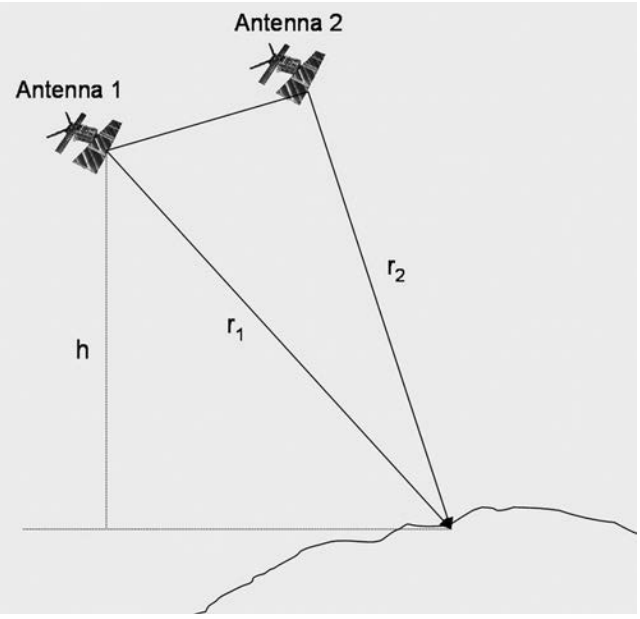

Fig. 1 - Schematic view of InSAR geometry. Antenna 1 and Antenna 2 look at the target area, at distance r_1 and r_2, from the same sight angle. The satellite altitude is h.

twice. The former configuration is called single-pass interferometry, the latter is referred to as repeat-pass interferometry. In the repeat-pass configuration, the temporal baseline is the time difference between the acquisitions. This latter configuration is the more reliable for the measurment of the effects of natural disasters that generate surface displacements, such as earthquakes, volcanic eruptions, landslides. Hydrology, Geology, Geomorphology, Seismology, Volcanology, Environmental pollution are thus the main topics to which InSAR conributed.

The interferogram is the combination of the signals S_1 and S_2 received at Antenna 1 and 2 respectively (Fig. 1). More precisely be:

$$S_1 = A_1 e^{-j\frac{4\pi r_1}{\lambda}} \quad S_2 = A_2 e^{-j\frac{4\pi r_2}{\lambda}}$$

where A_1 and A_2 are the amplitudes and λ is the wavelength. The interferogram is the difference of the phase component and is the product of S_1 versus the complex conjugate of

$$S_2, S_1 \cdot S_2^* = A_1 \; A_2 e^{-j\frac{4\pi(r_1 - r_2)}{\lambda}} .$$

Therefore, the interferometric phase φ_{int} can be schematically split into five terms:

$$\varphi_{\text{int}} = \varphi_f + \varphi_{topo} + \varphi_{displ} + \varphi_{atm} + \varphi_{err}$$

where φ_f is the flat Earth component (the orbital phase), the topographic phase is φ_{topo}, the displacement phase is φ_{displ}, the atmospheric term φ_{atm} and the error phase φ_{err}. Except for this latter and the φ_f, each term contains information relevant to specific issues. The

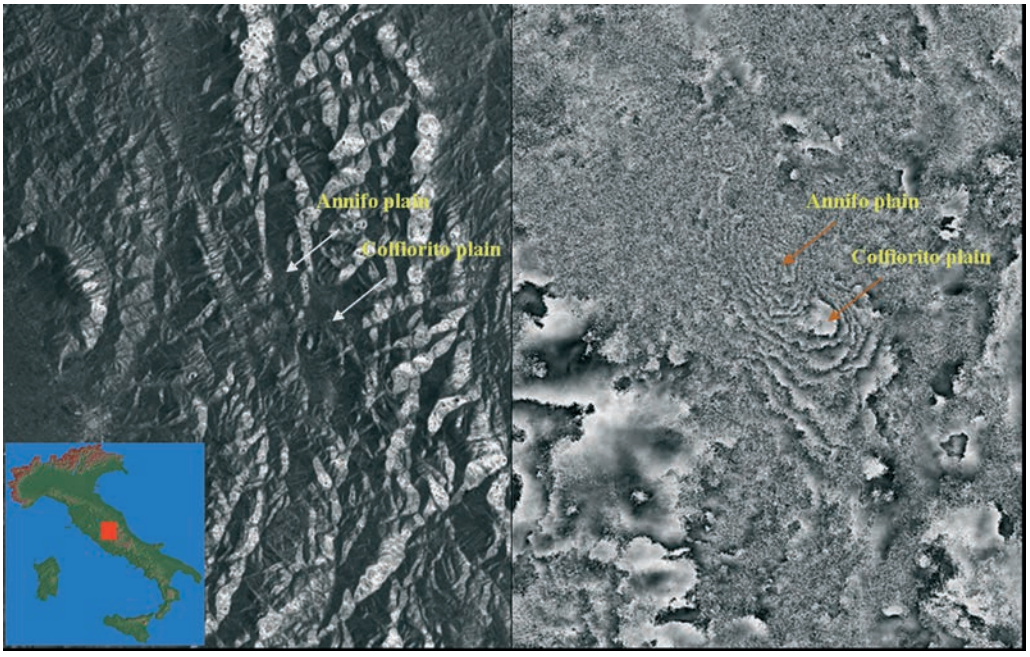

Fig. 2 - The Umbria-Marche earthquake: a) amplitude SAR image of the epicentral area. The Colfiorito plain and the Annifo plain are also shown; b) co-seismic interferogram of the epicentral area. The surface displacement pattern is represented by differential fringes, each corresponding to a LOS distance change of about 2.8 cm (i.e. $\frac{\lambda}{2}$). InSAR measured about 14 cm subsidence within the Colfiorito plain and about 25 cm in the Annifo plain.

$\varphi = \frac{4\pi}{\lambda}\Delta R$ is the phase component that accounts for the satellite-to-target distance change ΔR.

2.1. Case studies

Since the Landers earthquake, InSAR has been used on a huge number of other earthquakes, to provide the displacement pattern over all the epicentral region and to measure the co-seismic surface deformation: Northridge, California, 1994 (Massonnet, *et al.,* 1996; Murakami *et al.,* 1996); Kobe, Japan, 1995 (Ozawa *et al*., 1997); Grevena, Greece, 1995 (Meyer *et al.,* 1996); Antofogasta, Chile, 1995 (Pritchard *et al.,* 1998); Kagoshima-Kenhokuseibu, Japan, 1997 (Fujiwara *et al.,* 1998a); Umbria-Marche, Italy, 1997 (Stramondo *et al*., 1999) (Fig. 2), Izmit, Turkey, 1999 (e.g. Reilinger *et al*., 2000; Feigl *et al*., 2002), Bam, Iran, 2003 (Talebian *et al*., 2004; Stramondo *et al*., 2005) (Fig. 3).

The above-mentioned cases are just some meaningful examples of the InSAR co-seismic analysis performed since 1992. For instance, the 1997 Umbria-Marche seismic sequence is the first example of an InSAR analysis in Italy (Fig. 2). Three co-seismic interferograms have been computed to study the evolution of the surface displacement pattern due to as many mainshocks (Lundgren and Stramondo, 2002). The interferogram in Fig. 2b shows the differential phase φ_{displ} in the style of fringes. The term fringe indicates a complete phase cycle ($-\pi$ to $+\pi$) and corresponds to the satellite-to-target distance change equal to $\frac{\lambda}{2}$ (whereas λ=5.66 cm for C-Band

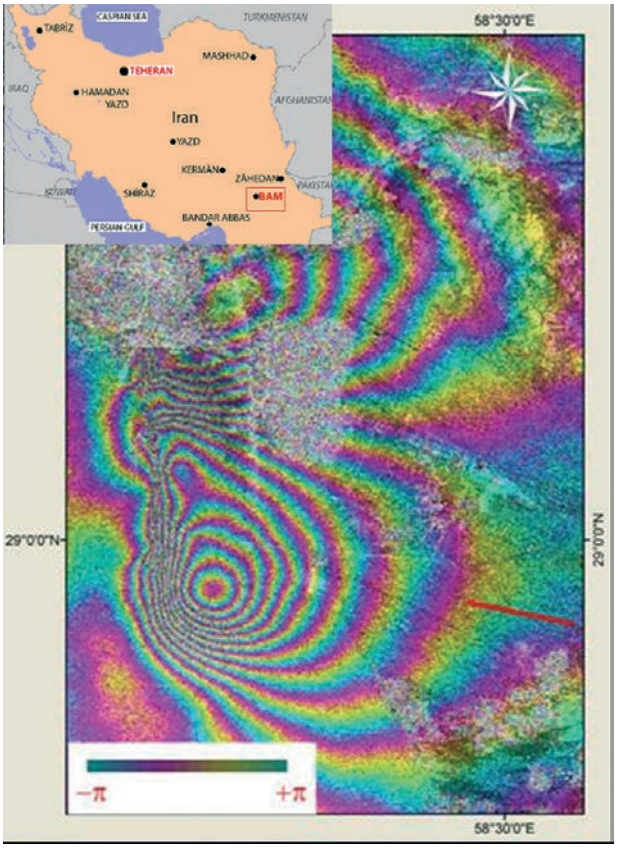

Fig. 3 - The 2003 Bam earthquake: co-seismic interferogram of the epicentral area. The surface displacement pattern is represented by differential fringes. This is the first InSAR application exploiting the capabilities of the Envisat ASAR sensor.

sensors). InSAR measured a few centimeter displacements along the LOS and a maximum of about 25 cm within the Annifo Valley (Stramondo *et al*., 1999).

Concerning the 2003 Bam earthquake, this is the first seismological use of the new ESA Envisat-ASAR sensor (Fig. 3) that has replaced the former European satellites, ERS1 and ERS2.

The inflation and deflation of the Mount Etna edifice before and after the eruption, is one of the former cases of volcanic application of InSAR in volcanology (Massonnet *et al*., 1995). Afterwards, a number of volcano deformation studies provided some promising results. These include investigations of several active Alaskan volcanoes (Lu *et al*., 1997; Lu and Freymueller, 1998), rifting and volcanism in Iceland (Sigmundsson *et al*., 1997; Vadon and Sigmundsson, 1997), localized inflation on Izu Peninsula, Japan (Fujiwara *et al*., 1998b), dike intrusions in the Fernandina volcano, Galapagos (Jónsson *et al*., 1999) and Piton de la Fournaise volcano on La Reunion Island (Sigmundsson *et al*., 1999), and deformation of the active calderas of Yellowstone (Wicks *et al*., 1998) and Long Valley (Thatcher and Massonnet, 1997).

3. Advanced InSAR (A-InSAR) techniques

The InSAR approach based on the interferometric of a single image pair is mainly effective for single deformation events characterized by centimetric displacements at least. Over the last few

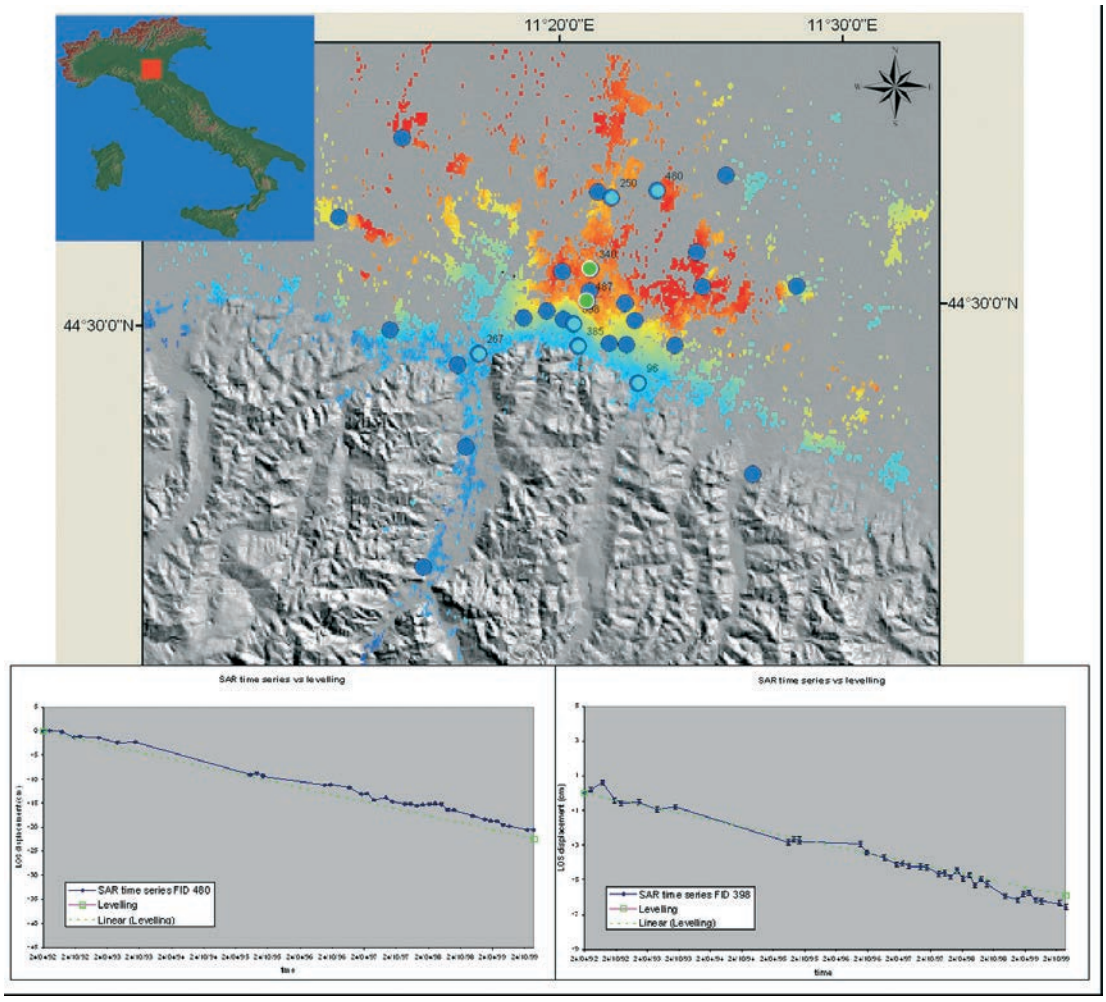

Fig. 4 - SBAS analysis of the surface deformation affecting the city of Bologna and the surrounding area. The SAR images cover the period 1992-2000. The InSAR detected deformation has been compared with the levelling data. Measurements at benchmark 340 and 398 (green circles) are plotted (dotted green line) with InSAR displacements (blue line).

years, new InSAR techniques, dealing with the combination of a large number of SAR data temporally distributed along a time span, have been developed. The A-InSAR techniques are generally able to provide an accurate measurement of the movement and are used to study the evolution of a surface deformation phenomenon. Therefore, they are also referred to as multitemporal InSAR techniques.

More generally, the A-InSAR allows us to provide a better estimate for each interferometric phase component. This is due to the increased capability to properly model the displacement phase contribution φ_{displ} and to follow its temporal and spatial changes. Furthermore, as the A-InSAR leads to computing a large number of interferograms, the topographic phase φ_{topo} is estimated several times. This approach provides a more accurate extraction of φ_{topo} and the possible topographic

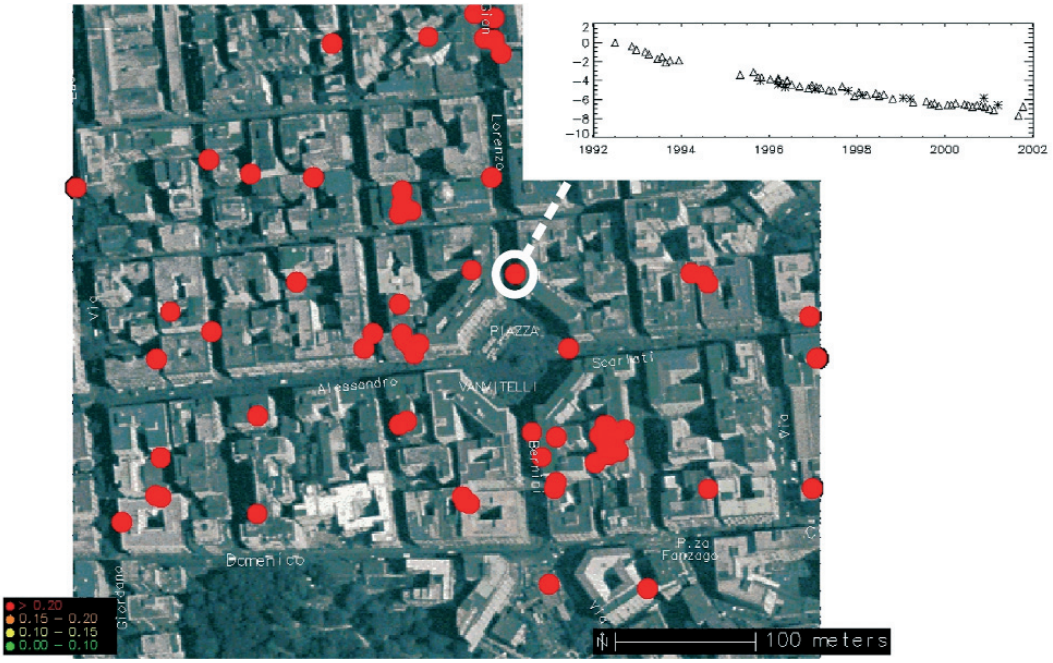

Fig. 5 - Full resolution SBAS technique. Comparison between leveling (stars) and DIFSAR (triangles) deformation time-series relevant to a building (identified by the white arrow) located in the maximum deformation area of the Vomero zone, shown in the picture (courtesy of Riccardo Lanari).

residuals are significantly reduced. The exact quantification of this latter component provides an improved displacement modelling and a more accurate geocoding. Finally, the A-InSAR techniques lead to the estimation of the atmospheric phase φ_{atm} within each interferogram. The atmospheric signal is spatially correlated and temporally decorrelated and thus the application of temporal and spatial filters allows us to remove it.

The A-InSAR processing is for computing the phase difference for those pixels whose backscattered signal is basically stable (coherent) along time. Therefore, the average surface deformation for each coherent pixel, i.e. the velocity map, is estimated and the time series showing the displacement for each pixel and for each interferogram is computed.

As far as the A-InSAR technique is concerned it can simply be classified according to the image selection criterion. Two main approaches are used:

- the image pairs coherence degree,
- the SAR amplitude stability.

The coherence γ is a typical InSAR quality parameter and provides the degree of statistical similarity of two complex signals:

$$\gamma = \frac{\left|E\left(S_1 S_2^*\right)\right|}{\sqrt{E\left(S_1 S_1^*\right)E\left(S_2 S_2^*\right)}}$$

Fig. 6 - PS analysis of the New Orleans area during the three years before the hurricane Katrina caused the flooding. The Radarsat PS revealed that the levees were in subsidence (courtesy of Alessandro Ferretti).

where E() is the ensemble average.

The SAR amplitude is the surface reflectivity and remains stable whereas the scatterers are unchanged. According to the previous schematic selection criterion the following multitemporal InSAR techniques belong to the first class: Small BAseline Subsets (SBAS) (Berardino *et al*., 2002; Lanari *et al*., 2004); CPT-Coherent Point Targets (Mora *et al*., 2003); InSAR Persistent Scatterers (Hooper *et al*., 2004).

Furthermore, the PS-Permanent Scatterers (Ferretti *et al*., 2000), the IPTA-Interferometric Point Target Analysis (Werner *et al*., 2003) and the SPN-Stable Point Network (Crosetto *et al*., 2005) rely on the selection of those pixels behaving as persistent scatterers.

Advantages and disadvantages for both approaches can be briefly summarized. Those dealing with the coherence degree are more suitable for application in regions with higher long-term coherence. Moreover, as the coherence is computed within a certain area (a spatial window), whenever such area is decorrelated, except for a coherent pixel, this latter will have a low coherence value.

The stable-amplitude methods have the advantage of exploiting all the coherent pixels of the image. Therefore, a single persistent pixel outside the coherent area is also considered. The effective use of A-InSAR techniques is prone to the availability of a huge number of SAR images and their continuity over large periods. The temporal coverage is a key issue for those applications aimed at detecting slow deformation rates and providing a reliable monitoring tool.

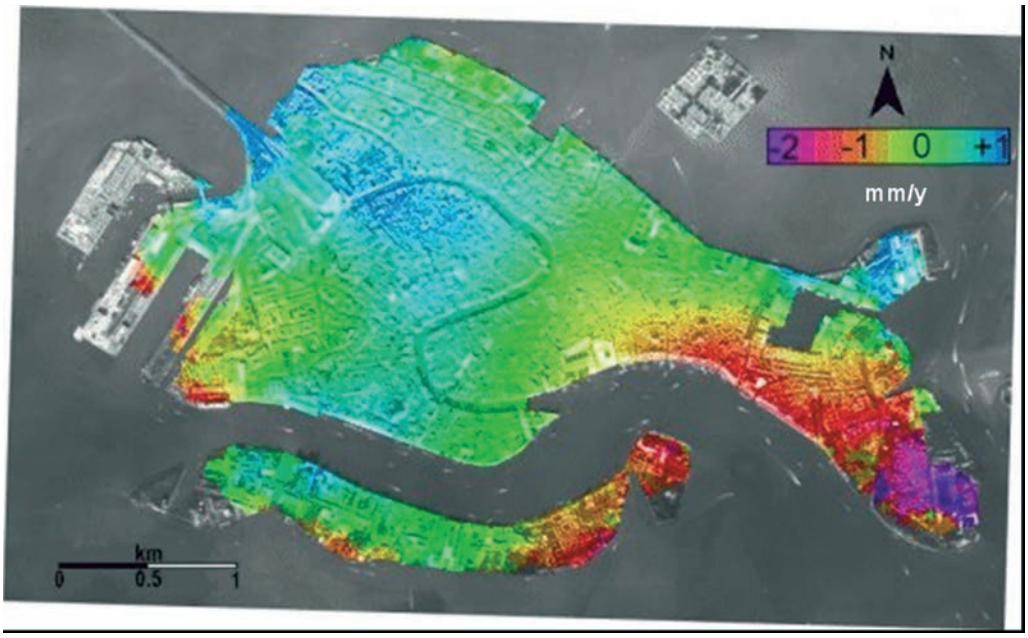

Fig. 7 - IPTA analysis of the city of Venice. During 1992-1996 IPTA revealed fairly stable conditions along the area with few mm/y movements.

3.1. Case studies

The A-InSAR techniques provide a high accuracy and high-precision measurements comparable with those of geodetic techniques. Therefore, an important issue is the validation of A-InSAR with ground surveys, topographic levelling and GPS. In this topic, Casu *et al*. (2006) compared the results of the application of the SBAS technique with the displacements from levelling campaigns. To reduce the error 116 SAR images were used, half from ascending and half from descending paths. The 290 benchmarks of the Somma-Vesuvio volcano area have been measured and compared with InSAR results. The $\sigma \cong 1$ mm/y of the differences between the levelling measure projected onto the LOS and the InSAR means a very high correlation and agreement.

Whenever talking about SBAS, we refer to the new algorithm for the analysis of slow deformation exploiting the combination of small-baseline interferograms proposed in Berardino *et al*. (2002). The SBAS technique computes a huge amount of interferograms and later performs the connections among them. This allows an accurate estimation of the deformation and, parallelly, cancels the atmospheric and topographic residuals.

In Stramondo *et al*. (2007) a further application to demonstrate the effectiveness of SBAS is described. The surface displacement in and around the city of Bologna (Fig. 4) has been measured by SBAS and compared with about 500 levelling measurements. Based on external data, as the geological and hydrogeological settings, the InSAR retrieved deformation pattern allowed us to make the hypothesis of two possible causes, natural (tectonic) and anthropogenic. The subsidence rates are from few mm/y to 59 mm/y in the 1992-2000 time period and the standard deviation of the differences between the levelling measure projected onto the LOS and the InSAR is $\sigma \cong 2$ mm/y.

Further achievements lead us to analyze the deformation at full resolution scale and to provide the deformation map affecting the single building. A recent application investigated the urban subsidence in Naples (Lanari *et al*., 2004), focusing on the Vomero and the Campi Flegrei areas (Fig. 5) where the density of coherent points is about 250 points/km^2. The SBAS demonstrated its capabilities to provide the monitoring of buildings.

The Permanent Scatterers (PS) algorithm proposed by Ferretti *et al*. (2000) is specifically addressed for the full exploitation of the electromagnetic properties of stable scatterers. We refer to PSs as to independent radar-bright and radar-phase stable points detected along the overall SAR scene. The technique specifically monitors the motion of single buildings, outcrops, at a level of about 1 mm/y. A recent application over the San Francisco Bay area was aimed at measuring the surface effects due to active tectonics and hydrologic processes. Furthermore, the PS results have been integrated with precise horizontal measurements from GPS (Ferretti *et al*., 2004) to validate the detected motion. In Dixon *et al*. (2006), the PS technique offered an analysis of the subsidence in New Orleans in the years prior the catastrophic flooding of 2005. The study revealed that the city underwent rapid subsidence in the three years before hurricane Katrina of August 2005 (Dixon *et al*., 2006). The PS analysis (Fig. 6) based on Radarsat images indicated that since their construction the levees were affected by a subsidence of more than 1 m thus favouring the disaster.

The IPTA is a further technique exploiting the stable point-like scatterer properties (Werner *et al*., 2003). IPTA has been used to detect and monitor the motion of single buildings, urban areas and slope stability. An interesting application was the monitoring of the worldwide famous and historical city of Venice from 1992 to 1996 (Tosi *et al*., 2002). The result is reassuring, being the subsidence rates in the order of a few mm/y (Fig. 7).

4. Conclusion

In fifteen years or more InSAR has become an effective, useful and absolutely necessary tool for Earth surface deformation studies. Seismology and Volcanology, benefited from the use of InSAR, but it is also used for environmental studies, landslides and urban subsidence. The recent improvements of signal processing methods provided geophysicists a further instrument for slow deformations. And it is noteworthy how the potentialities of InSAR and A-InSAR have been anticipated by Gabriel *et al*. (1989) who concluded their paper with the following sentence: "The possibilities include...to monitor long-term motion, possibly resulting in earthquake predictions". The latter statement can be considered the next frontier to overcome.

REFERENCES

Amelung F., Galloway D.L., Bell J.W., Zebker H.A. and Laczniak R.J.; 1999: *Sensing the ups and downs of Las Vegas: InSAR reveals structural control of land subsidence and aquifer-system deformation*. Geology, **27**, 483-486.

Berardino P., Fornaro G., Lanari R. and Sansosti E.; 2002: *A new Algorithm for Surface Deformation Monitoring based on Small Baseline Differential SAR Interferograms.* IEEE Trans on Geosci. and Remote Sensing, **40**, 2375-2383.

Casu F., Manzo M. and Lanari R.; 2006: *A quantitative assessment of the SBAS algorithm performance for surface deformation retrieval from DInSAR data*. Remote Sensing of Environment, **102**, 195-210.

Crosetto M., Crippa B. and Biescas E.; 2005: *Early detection and in-depth analysis of deformation phenomena by radar*

interferometry. Engineering Geology, **79**, 81-91.

Curlander J.C. and McDonough R.N.; 1991: *Synthetic Aperture Radar: systems and signal Processing.* Wiley, New York, 647 pp.

Dixon T.H., Amelung F., Ferretti A., Novali F., Rocca F., Dokkas R., Sella G., Kim S.W., Wdowinski S. and Whitman D.; 2006: *Subsidence and flooding in New Orleans.* Nature, **441**, 587-588.

Elachi C.; 1988: *Spaceborne Radar Remote Sensing: applications and techniques.* IEEE, New York, 255 pp.

Feigl K.L., Sarti F., Vadon H., McClusky S., Ergintav S., Durand P., Bürgmann R., Rigo A., Massonnet D. and Reilinger R.; 2002: *Estimating slip distribution for the Izmit mainshock from coseismic GPS and INSAR measurements.* Bull. Seism. Soc. Am., **92**, 138-160.

Ferretti A., Prati C. and Rocca F.; 2000: *Non-linear subsidence rate estimation using permanent scatterers in differential SAR Interferometry.* IEEE Trans. Geosci. Remote Sensing, **38**, 2202-2212.

Ferretti A., Novali F., Bürgmann R., Hilley G. and Prati C.; 2004: *InSAR permanent scatterer analysis reveals ups and downs in San Francisco Bay Area.* Eos, **85**, 317-324.

Fujiwara S., Yarai H., Ozawa S., Tobita M., Murakami M., Nagakawa H., Nitta K., Rosen P.A. and Werner C.L.; 1998a: *Surface displacement of the March 26, 1997 Kagoshima- Kenhokuseibu earthquake in Japan from synthetic aperture radar interferometry*. Geophys. Res. Lett., **25**, 4541-4544.

Fujiwara S., Rosen P.A., Tobita M. and Murakami M.; 1998b: *Crustal deformation measurements using repeat-pass JERS 1 synthetic aperture radar interferometry near the Izu Peninsula, Japan*. J. Geophys. Res., **103**, 2411-2426.

Gabriel A., Goldstein R. and Zebker H.; 1989: *Mapping small elevation changes over large areas: differential radar interferometry.* J. Geophys. Res., **94**, 9183–9191.

Galloway D.L., Hudnut K.W., Ingebritsen S.E., Phillips S.P., Peltzer G., Rogez F. and Rosen P.A.; 1998: *Detection of aquifer system compaction and land subsidence using interferometric synthetic aperture radar.* Antelope Valley, Mojave Desert, California. Water Resources Research, **34**, 2573-2585.

Hooper A., Zebker H., Segall P. and Kampes B.; 2004: *A new method for measuring deformation on volcanoes and other natural terrains using InSAR persistent scatterers.* Geophys. Res. Lett., **31**, L23611. doi:10.1029/2004GL021737.

Jónsson S., Zebker H.A., Cervelli P., Segall P., Garbeil H., Mouginis-Mark P. and Rowland S.; 1999: *A shallow-dipping dike fed the 1995 flank eruption at Fernandina Volcano, Galapagos, observed by Satellite radar interferometry*. Geophys. Res. Lett., **26**, 1077-1080.

Lanari R., Mora O., Manunta M., Mallorqui J., Berardino P. and Sansosti E.; 2004: *A small baseline approach for investigating deformations on full resolution differential SAR interferograms.* IEEE Transactions on Geoscience and Remote Sensing, **42**, 1377-1386.

Lu Z., Fatland R., Wyss M., Li S., Eichelberer J., Dean K. and Freymueller J.T.; 1997: *Deformation of New Trident volcano measured by ERS-1 SAR interferometry, Katmai National Park, Alaska.* Geophys. Res. Lett. **24**, 695-698.

Lu Z. and Freymueller J.T.; 1998: *Synthetic aperture radar interferometry coherence analysis over Katmai volcano group, Alaska.* J. Geophys. Res. **103**, 29887-29894.

Lundgren P. and Stramondo S.; 2002: *Slip distribution of the 1997 Umbria-Marche earthquake sequence through joint inversion of GPS and DInSAR data*. J. Geophy. Res., **107**, B11, 2316, doi:10.1029/2000JB000103.

Massonet D., Rossi M., Carmona C., Adragna F., Peltzer G., Feigl K. and Rabaute T.; 1993: *The displacement field of the Landers earthquake mapped by radar interferometry.* Nature, **364**, 138-142.

Massonet D., Briole P. and Arnaud A.; 1995: *Deflation of Mount Etna monitored by spaceborne radar interferometry.* Nature, **375**, 567-570.

Massonnet D., Feigl K.L., Vadon H. and Rossi M.; 1996: *Coseismic deformation field of the Mw 6.7 Northridge, California earthquake of January 17, 1994 recorded by 2 radar satellites using interferometry.* Geophys. Res. Lett., **23**, 969-972.

Massonnet D., Holzer T. and Vadon H.; 1997: *Land subsidence caused by the East Mesa geothermal field, California, observed using SAR interferometry.* Geophys. Res. Lett., **24**, 901–904.

Meyer B., Armijo R., Massonnet D., Dechabalier J.B., Delacourt C., Ruegg J.C., Acache J., Briole P. and Papanastassiou D.; 1996: *The 1995 Grevena (Northern Greece) earthquake-fault model constrained with tectonic observations and SAR interferometry*. Geophys. Res. Lett., **23**, 2677-2680.

Mora O., Mallorquí J. J. and Broquetas A.; 2003: *Linear and nonlinear terrain deformation maps from a reduced set of interferometric SAR images.* IEEE on Transaction Geoscience and Remote Sensing, **41**, 2243-2253.

Murakami M., Tobita M., Fujiwara S., Saito T. and Masaharu H.; 1996: *Coseismic crustal deformations of 1994 Northridge, California, earthquake detected by interferometry.* J. Geophys. Res., **101**, 8605-8614.

Ozawa S., Murakami M., Fujiwara S. and Tobita M.; 1997: *Synthetic aperture radar interferogram of the 1995 Kobe earthquake and its geodetic inversion.* Geophys. Res. Lett., **24**, 2327-2330.

Peltzer G. and Rosen P.; 1995: *Surface displacements of the 17 May 1993 Eureka Valley, California, earthquake observed by SAR interferometry.* Science, **268**, 1333-1336.

Pritchard M., Simons M., Lohman R., Chapin E., Rosen P.A. and Webb F.H.; 1998: *Constraints on crustal deformation in northern Chile using interferometric synthetic aperture radar*. EOS Trans. AGU, **79**, 184 (Abstr.).

Reilinger R.E., Ergintav S., Bürgmann R., McClusky S., Lenk O., Barka A., Gurkan O., Hearn L., Feigl K.L., Cakmak R., Aktug B., Ozener H. and Toksöz M.N.; 2000: *Coseismic and postseismic fault slip for the 17 August 1999, M 7.4, Izmit, Turkey earthquake.* Science, **289**, 1519–1524.

Salvi S., Atzori S., Tolomei C., Allievi J., Ferretti A., Rocca F., Prati C., Stramondo S. and Feuillet N.; 2004: *Inflation rate of the Colli Albani volcanic complex retrieved by the permanent scatterers SAR interferometry technique.* Geophys. Res. Lett., **31**, L12606.

Sigmundsson F., Vadon H. and Massonnet D.; 1997: *Readjustment of the Krafla spreading segment to crustal rifting measured by satellite radar interferometry*. Geophys. Res. Lett., **24**, 1843-1846.

Sigmundsson F., Durand P. and Massonnet D.; 1999: *Opening of an eruptive fissure and seaward displacement at Piton de la Fournaise volcano measured by RADARSAT satellite radar interferometry.* Geophys. Res. Lett., **26**, 533-536.

Stramondo S., Tesauro M., Briole P., Sansosti E., Salvi S., Lanari R., Anzidei M., Baldi P., Fornaro G., Avallone A., Buongiorno M.F., Franceschetti G. and Boschi E.; 1999: *The September 26, 1997 Colfiorito, Italy, earthquakes: modeled coseismic surface displacement from SAR interferometry and GPS.* Geophys. Res. Lett., **26**, 883-886.

Stramondo S., Moro M., Tolomei C., Cinti F.R. and Doumaz F.; 2005: *InSAR surface displacement field and fault modelling for the 2003 Bam earthquake (southeastern Iran)*. Journal of Geodynamics, doi: 10.1016/j.jog. 2005.07.013.

Stramondo S., Saroli M., Tolomei C., Moro M., Doumaz F., Pesci A., Loddo F., Baldi P. and Boschi E.; 2007: *Surface movements in Bologna (Po Plain - Italy) detected by multitemporal DInSAR.* Remote Sensing of Environment, doi:10.1016/j.rse.2007.02.023.

Talebian M., Fielding E.J., Funning G.J., Ghorashi M., Jackson J., Nazari H., Parsons B., Priestley K. and Rosen P.A.; 2004: *The 2003 Bam (Iran) earthquake: Rupture of a blind strike-slip fault.* Geophys. Res. Lett., **31**, L11611, doi:10.1029/2004GL020058.

Thatcher W. and Massonnet D.; 1997: *Crustal deformation at Long Valley Caldera, eastern California, 1992–1996 inferred from satellite radar interferometry*. Geophys. Res. Lett., **24**, 2519-2522.

Tosi L., Carbognin L., Teatini P., Strozzi T. and Wegmüller U.; 2002: *Evidence of the present relative land stability of Venice, Italy, from land, sea, and space observations.* Geophys. Res. Lett., **29**, 10.1029/2001GL013211.

Usai S.; 2003: *A least squares database approach for SAR interferometric data.* IEEE Transactions on Geoscience and Remote Sensing, **41**, 753-760.

Vadon H. and Sigmundsson F.; 1997: *Crustal deformation from 1992 to 1995 at the Mid- Atlantic ridge, southwest Iceland, mapped by satellite radar interferometry*. Science, **275**, 193-197.

Werner C., Wegmuller U., Strozzi T. and Wiesmann A.; 2003: *Interferometric point target analysis for deformation mapping.* Proceedings IEEE International. Geoscience and Remote Sensing Symposium, 2003. Vol. 7, pp. 4362-4364.

Wicks C., Thatcher W. and Dzurisin D.; 1998: *Migration of fluids beneath Yellowstone caldera inferred from satellite radar interferometry.* Science, **282**, 458-462.

Corresponding author: Salvatore Stramondo
INGV - Istituto Nazionale di Geofisica e Vulcanologia, Roma
Centro Nazionale Terremoti
Via di Vigna Murata 605, 00143 Roma, Italy
phone: +39 06 51860521; fax: +39 06 5041181; e-mail: stramondo@ingv.it